Matter-antimatter asymmetries at LHCb - development of a 3rd year lab project

Jose Gutierrez 7618322

May 11, 2014

School of Physics and Astronomy

The University of Manchester

Mphys Report

Abstract

The goal is to set the foundations for a new third year lab experiment in particle physics data analysis. To this end, B meson three-body decays $B^{\pm} \to K^{\pm}\pi^{+}\pi^{-}$, $B^{\pm} \to K^{\pm}K^{+}K^{-}$ and $B^{\pm} \to \pi^{\pm}\pi^{+}\pi^{-}$ where studied from data collected by LHCb to look for matter-antimatter asymmetries. In this context, charmless decays were analysed, which offer interference patterns between two-body resonances in the Dalitz plots and hence the study of CP violation. The global charge asymmetries of these modes are measured as -0.053 ± 0.007 ($B^{\pm} \to K^{\pm}K^{+}K^{-}$), 0.066 ± 0.023 ($B^{\pm} \to \pi^{\pm}\pi^{+}\pi^{-}$) and -0.001 ± 0.011 ($B^{\pm} \to K^{\pm}\pi^{+}\pi^{-}$). The significance of the asymmetry observed in $B^{\pm} \to K^{\pm}K^{+}K^{-}$ decay channel exceeds three standard deviations as an evidence of CP asymmetry in charmless three-body B decays. In addition to the global CP asymmetries, larger and significant asymmetries are observed in localized regions of phase space.

Contents

1 Introduction **3**
1.1 Theoretical Introduction . . . 3
1.1.1 Symmetries . . . 3
1.1.2 CP Violation in the Standard Model . . . 3
1.2 The LHCb Experiment . . . 7

2 Data Analysis **9**
2.1 Selection Cuts . . . 9
2.2 Global Asymmetries . . . 10
2.3 Resonances . . . 11
2.4 Regional Asymmetries . . . 13

3 Laboratory experiment development **17**

4 Discussion **17**

5 Conclusions **18**

A Dalitz Plots **21**

1 Introduction

CP Violation is an important subject to the understanding of particle physics and the early universe. It is the suggested main mechanism for the observed matter antimatter asymmetries in the universe. In the Standard Model, CP Violation originates from the weak interactions of quarks and leptons, to date, this has only been observed in the quark sector, such as the decays of charged B mesons. [1]

1.1 Theoretical Introduction

According to the Standard Model, quarks can interact strongly (mediated by gluons), they are never isolated in nature but always bound in composite subatomic particles called hadrons (due to confinement by gluon fields). In this category, mesons are formed by a quark and antiquark pair and have integer spin. Most relevant to this report are B mesons, which are composed of a b quark and other lighter quarks, e.g. $B^-(b\bar{u})$ and $B^+(\bar{b}u)$. An essential part of the Stardard Model is the concept of symmetry. The laws of physics are invariant under simple transformations of the coordinate system like a rotation. Violations of the expected symmetries of a theory play a crucial role in the understanding of particle physics. Most relevant to this report is the combined violation of the C and P symmetries. It turns out that B mesons are an excellent place to observe this phenomenon as the SM predicts large effects with high accuracy. CP violation has cosmological significance as it plays a crucial role in baryogenesis[1]. It is one of the Sakharov conditions[2]:

- Violation of the baryon number,
- C and CP violation,
- Interactions outside of thermal equilibrium, which set out the conditions necessary to produce an abundance of matter in the universe.

1.1.1 Symmetries

Symmetry is an important concept in any theory that describes a physical system since it results in conserved quantities, as stated by the Noether's theorem. In the Standard Model (SM), three discrete transformations can be defined:

- Parity (P): The parity operator reverses the spatial components of four-vectors, (t, x) $\rightarrow$ (t,$-$x). Changes momenta of particles by negative sign keeping spin invariant. Parity is implemented by a unitary operator P such that $P^2 = 1$, which requires its eigenstates to be equal to ± 1.
- Charge conjugation (C): Changes particles with their corresponding antiparticles. Both momentum and energy components are unchanged.
- Time reversal (T): Time reversal inverts the time axis only (t, x) $\rightarrow$ ($-$t, x).
- Chiral Symmetry: A non-Abelian symmetry, which is an exact symmetry in the limit of massless fermions. Left-handed and Right-handed parts of Dirac fields transform independently. The chiral symmetry transformation can be divided into a component that treats the left-handed and the right-handed parts equally, known as vector symmetry, and a component that actually treats them differently, known as axial symmetry. The γ_5 eigenvalue is called chirality. It is spontaneously broken as a dynamical effect of QCD interactions.

1.1.2 CP Violation in the Standard Model

In the Electroweak theory, $SU(2)_L \times U(1)$, part of the Standar Model, only left handed chiral components of fermionic fields interact weakly (and right handed anti-fermionic fields), the left handed chiral doublets are defined as [3]:

$$\begin{cases} t_3 = 1/2 \\ t_3 = -1/2 \end{cases} \quad \hat{q}_{Li} = \begin{pmatrix} \hat{u}_{Li} \\ \hat{d}_{Li} \end{pmatrix}, \text{Group } SU(2)_L \ ,$$

Where t_3 is the weak isospin quantum number, q_{Li} is the quark doublet in which the Li subscript goes from 1 to 3 indicating the quark generations. Since right hand chiral components do not interact weakly, it is assumed that all R-components are singlets under weak isospin group. The Yukawa quark lagrangian:

$$\mathcal{L}_{q\phi} = a_{ij}\bar{\hat{q}}_{Li}\hat{\phi}^{*}\hat{u}_{Rj} + b_{ij}\bar{\hat{q}}_{Li}\hat{\phi}\hat{d}_{Rj} + \text{ H.C. } ,$$

Where a_{ij} and b_{ij} are 3×3 complex coupling matrices, $\hat{u}_{Rj}$ and $\hat{d}_{Rj}$ are the right handed quark singlets, $\hat{\phi}$ is the Higgs field. After symmetry breaking, using the gauge:

$$\hat{\phi} = \begin{pmatrix} 0 \\ \frac{1}{\sqrt{2}}(v + \hat{H}) \end{pmatrix} ,$$

Where v is the vaccum spectation value and $\hat{H}$ is the physical Higgs field, the lagrangian then becomes:

$$\mathcal{L}_{q\phi} = -\left(1 + \frac{\hat{H}}{v}\right)[\bar{\hat{u}}_{Li}m^{u}_{ij}\hat{u}_{Rj} + \bar{\hat{d}}_{Li}m^{d}_{ij}\hat{d}_{Rj} + \text{ H.C.}] ,$$

In which $m^{u}_{ij} = -\frac{v}{\sqrt{2}}a_{ij}$ and $m^{d}_{ij} = -\frac{v}{\sqrt{2}}b_{ij}$ are the 'mass matrices' that can be made hermitian and diagonal by making unitary transformations on the generation triplets $\hat{u}_{Li}$ and $\hat{d}_{Li}$ by:

$$\hat{u}_{L\alpha} = (\hat{U}^{u}_{L})_{\alpha i)}\hat{u}_{Li} \qquad \hat{u}_{R\alpha} = (\hat{U}^{u}_{R})_{\alpha i)}\hat{u}_{Ri}$$

$$\hat{d}_{L\alpha} = (\hat{U}^{d}_{L})_{\alpha i)}\hat{d}_{Li} \quad \hat{d}_{R\alpha} = (\hat{U}^{d}_{R})_{\alpha i)}\hat{d}_{Ri} \ .$$

Now considering the $SU(2)_L \times U(1)$ gauge invariant interaction part of the lagrangian (In this case, showing just the charged current parts since they are related to the quark flavour change of quarks via charged $W^{\pm}$ bosons) written out in terms of the weak interaction fields:

$$\mathcal{L}_{qW} = i(\bar{\hat{u}}_{Lj}, \bar{\hat{d}}_{Lj})\gamma^{\mu}(\cdots + ig\tau \cdot \hat{\mathbf{W}}_{\mu}/2 + \dots)\begin{pmatrix} \hat{u}_{Lj} \\ \hat{d}_{Lj} \end{pmatrix} \ .$$

From the above lagrangian, the $\tau \cdot \hat{\mathbf{W}}_{\mu}/2$ term can be written as $\frac{1}{\sqrt{2}}(\tau_{+}\hat{W}_{\mu} + \tau_{-}\hat{W}^{*}_{\mu}) + \dots$, the operator $\hat{W}_{\mu}$ destroys W^{+} or creates W^{-}, the $\tau_{\pm}$ are the usual raising and lowering operators for the doublets. Hence the above lagrangian can be written as (considering just the W^{+} current term for simplicity):

$$-\frac{g}{\sqrt{2}}\bar{\hat{u}}_{L\alpha}[(\hat{U}^{u\dagger}_{L})_{\alpha j}(\hat{U}^{d}_{L})_{j\beta}]\gamma^{\mu}\hat{d}_{L\beta}\hat{W}_{\mu} + \text{H.C. } ,$$

where

$$V_{\alpha\beta} \equiv [\hat{U}^{u\dagger}_{L}\hat{U}^{d}_{L}]_{\alpha\beta} \ ,$$

is the non diagonal unitary CKM matrix. If there were only 2 quark doublets formed from u, d, c and s quarks, it would be possible to choose quark field phases such that a 2×2 matrix $V_{\alpha\beta}$ becomes orthogonal with real components. In such case, gauge interactions would conserve T and CP. For a 3×3 matrix transforming from mass basis to weak basis for 3 quark generations, there are 18 real parameters, but there are also 3 real diagonal conditions from unitarity and 3 complex off diagonal conditions, thus, leaving 9 real parameters. If the $V_{\alpha\beta}$ is taken to be real, that leaves an orthogonal rotation matrix parametrized by 3 Euler angles. Hence there are 6 phase parameters in the general unitary $V_{\alpha\beta}$, but there are 6 quark fields with 5 adjustable phase differences, which leaves just one irreducible phase degree of freedom after quark rephasing. This irreducible phase is responsible for CP violation in the quark sector. The relation between mass and weak eigenstates with CKM matrix:

$$\begin{pmatrix} d' \\ s' \\ b' \end{pmatrix} = \begin{pmatrix} V_{ud} & V_{us} & V_{ub} \\ V_{cd} & V_{cs} & V_{cb} \\ V_{td} & V_{ts} & V_{tb} \end{pmatrix}\begin{pmatrix} d \\ s \\ b \end{pmatrix} \tag{1}$$

Weak eigenstates = CKM matrix x Mass eigenstates. The CKM matrix is unitary, matrix elements are complex constants not determined by the standard model, but from experiment.

There is no unique parametrization of the CKM matrix, a standard one:

$$V = \begin{pmatrix} c_{12}c_{13} & s_{12}c_{13} & s_{13}e^{-i\delta} \\ -s_{12}c_{23} - s_{12}c_{23}s_{12}e^{-i\delta} & c_{12}c_{23} - s_{12}s_{23}s_{13}e^{-i\delta} & s_{23}c_{13} \\ s_{12}s_{23} - c_{12}c_{23}s_{13}e^{-i\delta} & -c_{12}s_{23} - s_{12}c_{23}s_{13}e^{-i\delta} & c_{23}c_{13} \end{pmatrix}$$

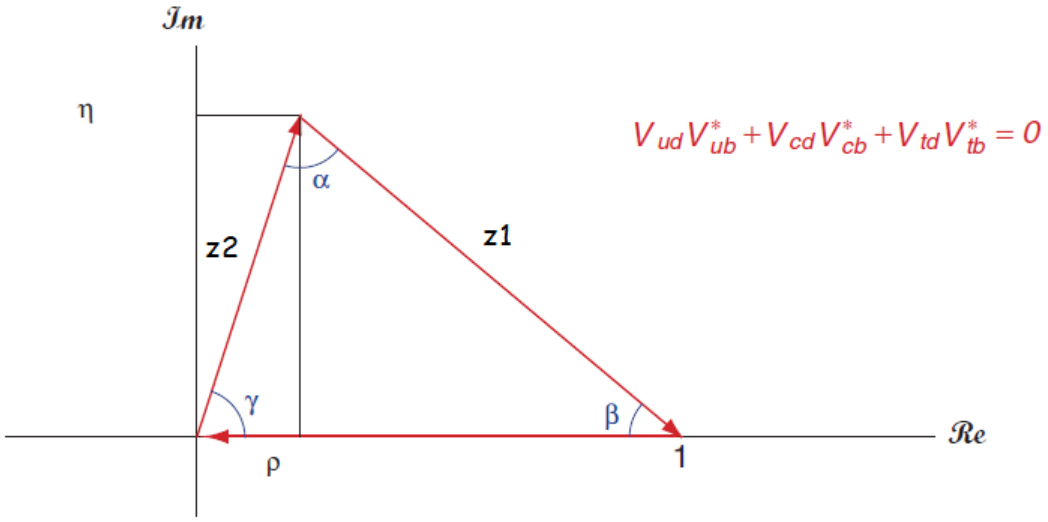

Figure 1: Unitary triangle in complex plane.

Where c_{ij} and s_{ij} are $\cos\theta_{ij}$ and $\sin\theta_{ij}$ rewill bespectively, θ_{ij} the Euler angles in orthogonal V and δ is the irreducicle CP violating phase. To have a measure independent of quark rephasing, consider on off-diagonal unitarity conditions:

$$V_{ud}V_{ub}^* + V_{cd}V_{cb}^* + V_{td}V_{tb}^* = 0$$

Since the best experimental measured factor is $V_{cd}V_{cb}^*$, divinding last expression by this:

$$z_2 + 1 + z_1 = 0$$

Represented in Figure 1. Now considering the condition above, with $s_{12} = \lambda$, $V_{cb} \simeq s_{12} = A\lambda^2$, $V_{ub} = s_{13}e^{-i\delta} = A\lambda^3(\rho - i\eta)$ and neglecting λ^4 terms, the CKM matrix can be written as (called Wolfenstein parametrization and λ as the Wolfenstein parameter):

$$V = \begin{pmatrix} 1-\lambda^2/2 & \lambda & A\lambda^3(\rho - i\eta) \\ -\lambda & 1-\lambda^2/2 & A\lambda^2 \\ A\lambda^3(1-\rho-i\eta) & -A\lambda^2 & 1 \end{pmatrix}$$

This suggests that CP violation is much more visible in B meson physics, which is studied here as direct CP violation in specific decay channels because of the coupling strengths involved in those decays ($A\lambda^3(\rho - i\eta)$ term), see Figure 2.

In Summary, CP violation in the Standard Model is described by irreducible complex phases in CKM matrices (Cabibbo-Kobayashi-Maskawa quark-mixing matrix). Weak eigenstates are different from mass eigenstates and are related by the CKM matrix.

There are 3 types of CP violation, indirect (mixing), direct (decays) and a third one as a combination of both. In this analysis, direct CP violation is relevant because $B^\pm \to K^\pm\pi^+\pi^-$, $B^\pm \to K^\pm K^+ K^-$ and $B^\pm \to \pi^\pm\pi^+\pi^-$ have common final states, see Figure 2 and 3. There are two types of phase in this process, weak phase due to weak interaction and strong phase from intermediate states. The source of strong phase in these processes is not well understood. Intermediate states are observed and studied in Dalitz plots (see appendix A), which are 2D histograms of squared mass of specific resultant pair particles from three body decays. One of these intermediate states J/Ψ contribution was removed to veto $J/\Psi \to \mu^+\mu^-$ as well as D^0 to remove charm contributions from 2 body invariant masses in decay channels studied in the present analysis, see Discussion.

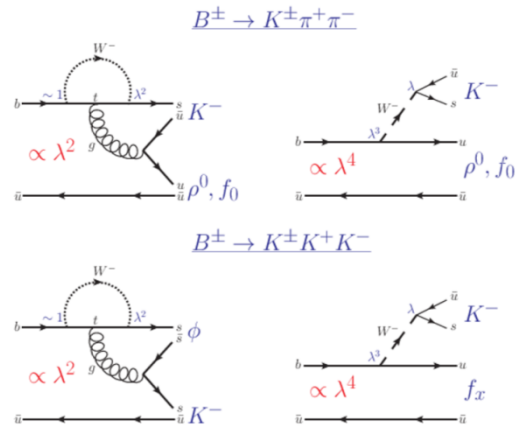

Figure 2: Tree and penguin SM diagrams for $B^\pm \to K^\pm\pi^+\pi^-$(top) and $B^\pm \to K^\pm K^+K^-$ (bottom). Where f_x holds for any resonance decaying into two kaons in the final state. Reproduced from [4].

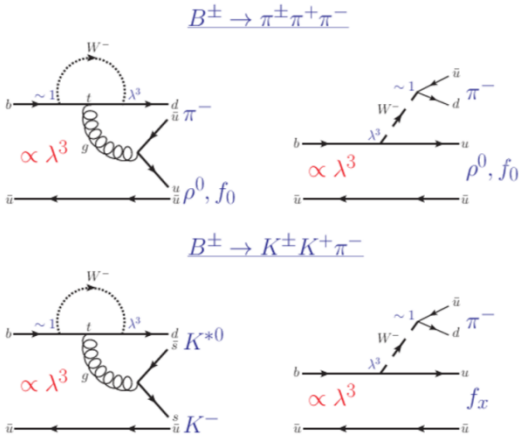

Figure 3: Tree and penguin SM diagrams for $B^\pm \to \pi^\pm\pi^+\pi^-$(top) and $B^\pm \to K^\pm K^+\pi^-$ (bottom). As before, f_x holds for any resonance decaying into two kaons in the final state. Reproduced from [4].

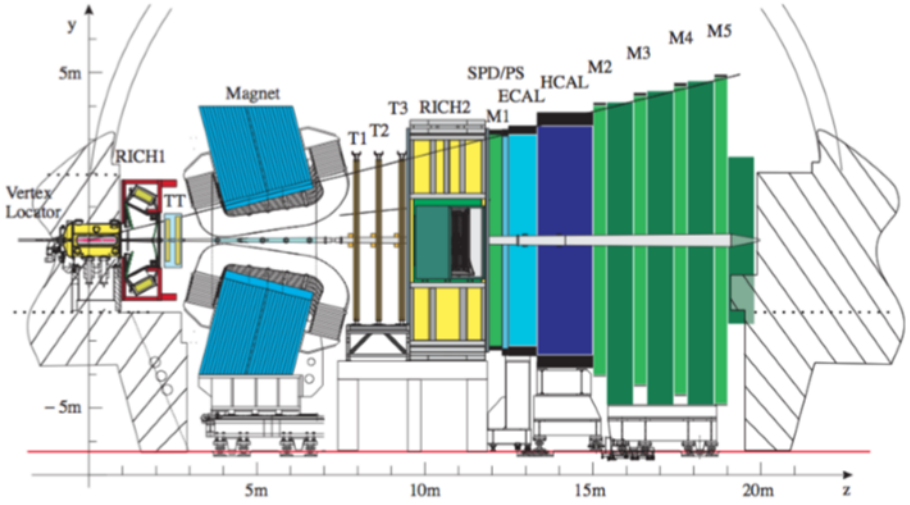

Figure 4: Schematic of the LHCb spectrometer. Sub-detectors are listed from interaction region (z = 0) towards the upstream region: Vertex Locator (VELO), RICH1, dipole magnet, Tracking stations (T1-3), RICH2, Scintillating Pad Detector (SPD), Calorimeter System (E/HCAL) and Muon System (M1-5), reproduced from [6].

1.2 The LHCb Experiment

The LHC is a proton-proton collider located at CERN with a designed centre-of-mass energy of 14 TeV and a luminosity of $10^{34} cm^{-2} s^{-1}$. The accelerator is divided in eight octants and beams circulate in opposite directions into two separate rings. Two separate rings, with opposite magnetic field, are required as the colliding particles carry the same charge. All superconductive magnets are cooled down to a temperature of 1.9 K, using superfluid helium, to operate them safely at magnetic fields up to 8.3T, depending on the energy of the beams. The high luminosity of the LHC is delivered through intense bunches consisting of 1.1×10^{11} protons each, separated by 50 ns intervals between each crossing.[5]

LHCb is an experiment dedicated to heavy flavour physics at the LHC. Its primary goal is to look for indirect evidence of new physics in CP violation and rare decays of bottom and charm hadrons. With the large $\bar{b}b$ production cross section of $\sim 500 \mu b$ expected at an energy of 14 TeV. With a modest luminosity of $2 \times 10^{32} cm^{-2} s^{-1}$ for LHCb, 10^{12} $\bar{b}b$ pairs would be produced in $10^{7} s$. It is primarily composed of a forward single arm spectrometer with 2 RICH detectors for particle identification, a dipole magnet, a precision silicon vertex detector.[5]

A charged particle going through a magnetic field experiences a force in the direction perpendicular to its motion, $F = q(v \times B)$. The radius, r, of the curvature is related to the strength of the magnetic field, B, and the particle momentum, P, via the relation:

$$r = \frac{P}{qB} \tag{2}$$

which comes from $F = q(v \times B)$, assuming perpendicular B to the direction of motion.

From equation 2, it is possible to obtain charge and momentum of a particle by measuring the direction and radius of the track curvature. The LHCb dipole magnet has an integrated magnetic field of $\int Bdl = 4(T.m)$ over 10m in the z-direction, see figure 4. An important feature of the dipole magnet is the ability to reverse the polarity of the magnetic field.

The LHCb tracking system consists of a set of sub-detectors that are used to reconstruct the trajectories of charged particles: a silicon-strip Vertex Locator (VELO) and a set of tracking stations. The VELO is used to reconstruct the primary vertices. The tracking detectors must have excellent spatial resolution for efficient reconstruction of particle trajectories. The tracking system comprises over $12m^2$ of silicon-strip detectors, see figure 5.

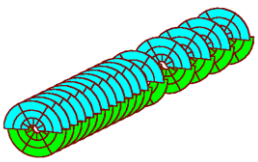

Figure 5: Series of disc detectors separated by 6mm.

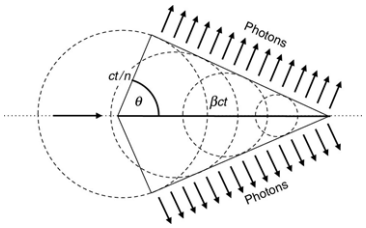

Figure 6: Schematic of the emission of Cherenkov radiation, reproduced from [1].

Bottom mesons have short lifetimes of approximately 1ps, which corresponds to typical flight distances from the primary vertex of approximately 1cm. To measure the position of these vertices, the VELO is located around the particle interaction region, 8mm from the beam and it consists of 88 silicon microstrip detectors.

Particle identification is needed to fully reconstruct decay channels. Typical particles that reach the PID detectors without decaying are pions, kaons, protons, muons and electrons. These are efficiently identified using the RICH detectors, the calorimeters and the muon system. Particles travelling in a material at a velocity faster than the speed of light will emit photons in a process called Cherenkov radiation. The photons are emitted in a cone centred on the particle trajectory.

$$\cos\theta = \frac{1}{n\beta} \tag{3}$$

Where θ is the angle at which radiation is produced (see figure 5), n is the refractive index of the material and β is v/c.

Using equation 3 and the measured momentum from the tracking system, the mass of the particle can be determined and it is particularly important to separate kaons and pions to reconstruct specific B-hadron decays. Particles with momentum in the range 2−65GeV/c are identified using the RICH1 detector, see figure 4. Particles with momentum up to approximately 100GeV/c are identified further downstream by the RICH2 detector.[5]

Variables	Selection cuts
Tracks P_T	> 0.1 GeV/c
Tracks P	> 1.5 GeV/c
Tracks IPχ^2	> 1
Tracks χ^2/n.d.f.	< 3
Sum of P_T of tracks	> 4.5 GeV/c
Sum of IPχ^2 of tracks	> 500
P_T of the highest-P_T track	> 1.5 GeV/c
$B^{\pm}$ candidate M_{KKK}	$5.05 - 6.30$ GeV/c^2
$B^{\pm}$ candidate IP χ^2	< 10
Secondary Vertex χ^2	< 12
Number of long tracks in the event	< 200

Figure 7: Pre applied cuts in data set recieved for analysis. Reproduced from [4].

Variable	Cut Value
PID Kaon	PIDK < -5
PID Pion	PIDK > 8
PID muon	PIDmu < 5
$B^{\pm}$ candidate PT	$> 1.7 GeV/c$
$B^{\pm}$ Flight Distance χ^2	> 700
PT of the highest-PT track	$> 1.5 GeV/c$
PT of the second highest-PT track	$> 0.9 GeV/c$
m($\pi\pi$) for J/ψ	$> 3.150, < 3.050 GeV/c$
m($\pi\pi$), m(Kπ), m(KK) for D^0	$> 1.894), < 1.834 GeV/c$

Table 1: Cuts made for the analysis

2 Data Analysis

From these detectors, data collected is arranged in Ntuples, which is a data structure containing events and relevant variables per event, like PID (particle ID), momentum (Px, Py, Pz), Total energy, etc. These variables are used in the present analysis; the most important of them in the selection of relevant events is PID.

2.1 Selection Cuts

The data received for this analysis had pre-applied cuts, these are shown in figure 7. After identifying premade cuts, a plot of invariant mass of B meson was produced for each decay channel, $B^{\pm} \to K^{\pm}\pi^{+}\pi^{-}$, $B^{\pm} \to K^{\pm}K^{+}K^{-}$ and $B^{\pm} \to \pi^{\pm}\pi^{+}\pi^{-}$ using equation 4 and relevant momentum and energy variables for each resultant particle of B meson decay.

$$M^2 = (\sum_{i}^{n} E_i) + (\sum_{i}^{n} \mathbf{P}_i) \tag{4}$$

Significant cuts were made to get sensible mass plots. The most important one is PID (more than 90% reduced events), since correct particle identification is essential to get relevant events for the analysis. Other variable cuts considered are transverse momentum and flight distance χ^2 of B meson since it has a short lifetime, also highest and second highest transverse momentum. Mass cuts around $\pm$ 30 MeV of J/ψ resonance (in $B^{\pm} \to K^{\pm}\pi^{+}\pi^{-}$, specifically in pair mass composed of $\pi\pi$ to get rid of muonic contributions) and D^0 mass to get rid of charm contributions (in all decay channels, specifically in pair masses composed of $\pi\pi$, Kπ and KK). All considered cuts are summarized in table 1.

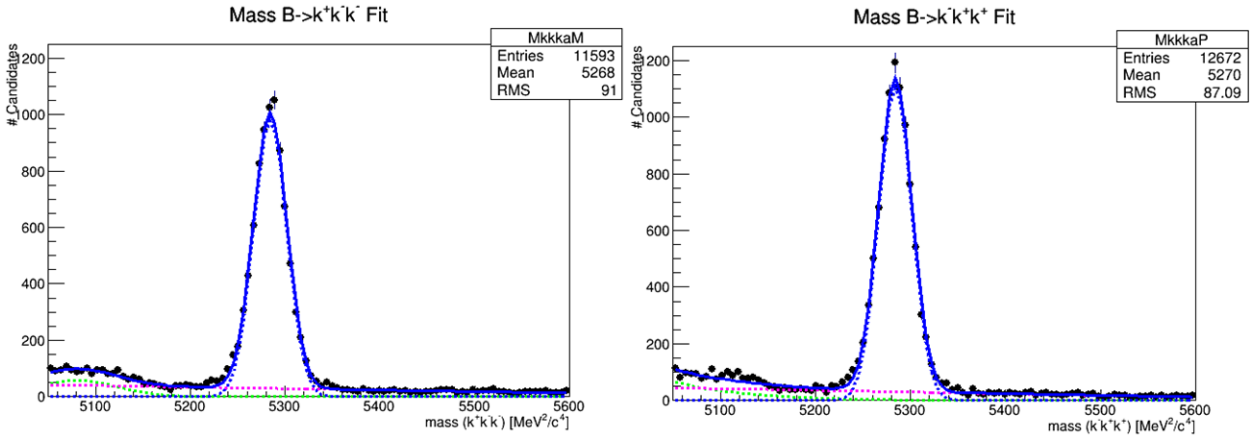

Figure 8: Invariant mass spectra of B meson in $B^{\pm} \to K^{\pm}K^{+}K^{-}$ decay channel. The left panel shows the B^{-} mode, and the right panel in each shows the B^{+} modes. Mass peak is shown as dotted blue line, combinatorial background as dotted magenta and partially reconstructed 4-body decays background as dotted green line.

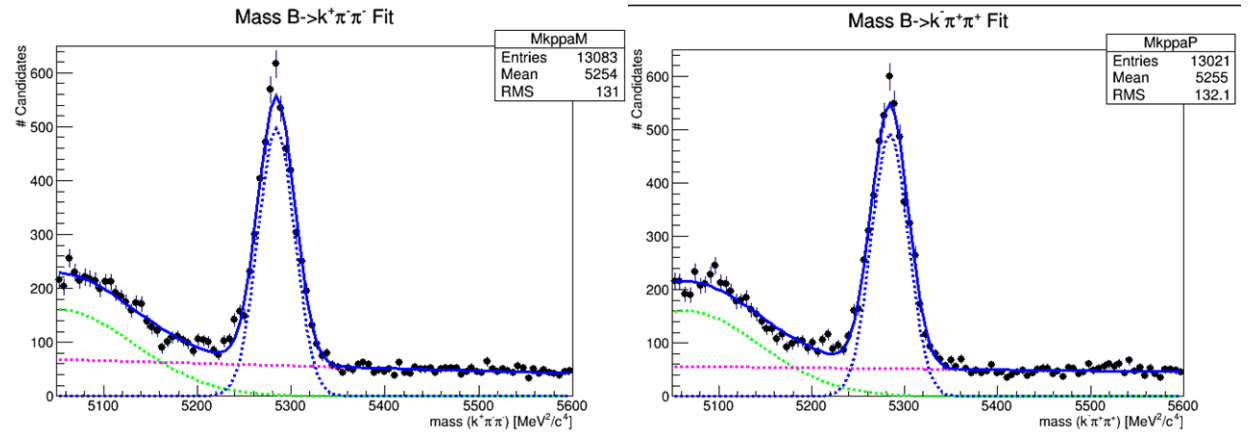

Figure 9: Invariant mass spectra of B meson in $B^{\pm} \to K^{\pm}\pi^{+}\pi^{-}$ decay channel. The left panel shows the B^{-} mode, and the right panel in each shows the B^{+} modes. Mass peak is shown as dotted blue line, combinatorial background as dotted magenta and partially reconstructed 4-body decays background as dotted green line.

2.2 Global Asymmetries

After cuts, fitting was done by using gaussian function to represent the main mass peak, another gaussian function for the 4-body decay background (to the left of the mass peak) and a 1st degree polynomial to represent combinatorial background (to the right of the mass peak). The resultant mass plots are shown in figure 8, 9 and 10 for each decay channel.

From fitting results, global asymmetries were calculated using:

$$Asy = \frac{N^{-} - N^{+}}{N^{-} + N^{+}} \tag{5}$$

where N is the number of signal events, taken from the integrated blue dotted line shown in figures 8, 9 and 10 using common standard gaussian integral,

$$\int_{-\infty}^{\infty} a\mathrm{e}^{-\frac{(x-b)^2}{2c^2}}\,\mathrm{d}x = ac\sqrt{2\pi}\ .$$

Errors were taken into account for the calculation of the integral and the asymmetry using the general error formulae:

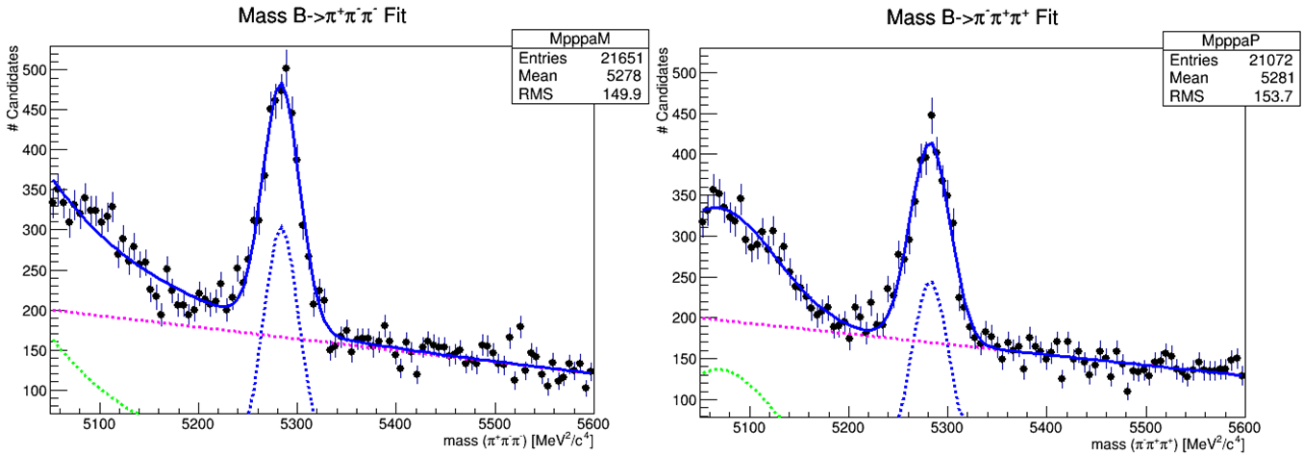

Figure 10: Invariant mass spectra of B meson in $B^{\pm} \to \pi^{\pm}\pi^{+}\pi^{-}$ decay channel. The left panel shows the B^{-} mode, and the right panel in each shows the B^{+} modes. Mass peak is shown as dotted blue line, combinatorial background as dotted magenta and partially reconstructed 4-body decays background as dotted green line.

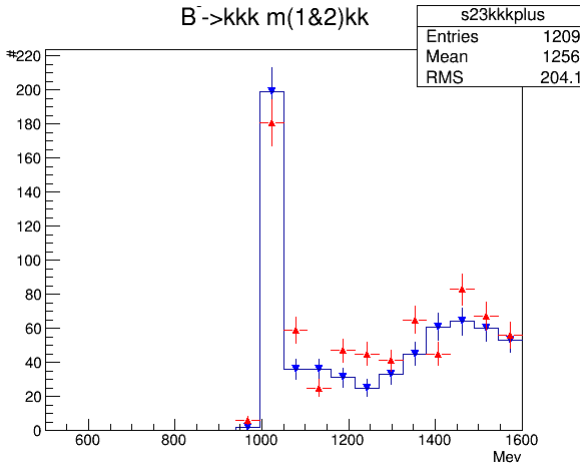

Figure 11: Low mass(kk) pair, $\phi(1020)$ resonance very clear as well as some small differences between B+ and B-. (Red triangle for B+ and blue triangle for B-).

$$\sigma^2_{total} = \left(\frac{\partial f}{\partial x}\right)^2 \sigma^2_x + \left(\frac{\partial f}{\partial y}\right)^2 \sigma^2_y + \ldots$$

The calculated global charge asymmetries obtained are -0.053 ± 0.007 ($B^{\pm} \to K^{\pm}K^{+}K^{-}$), 0.066 ± 0.023 ($B^{\pm} \to \pi^{\pm}\pi^{+}\pi^{-}$) and -0.001 ± 0.011 ($B^{\pm} \to K^{\pm}\pi^{+}\pi^{-}$).

2.3 Resonances

Invariant mass plots of intermediate states were also produced to identify resonances involved in each decay, in the case of $B^{\pm} \to K^{\pm}K^{+}K^{-}$ and $B^{\pm} \to \pi^{\pm}\pi^{+}\pi^{-}$ decay channels, intermediate states were produced by making separate plots for low mass and high mass pairs since all resultant particles are of the same type. These are shown in figures 11 and 12. In the case of $B^{\pm} \to K^{\pm}\pi^{+}\pi^{-}$, m($\pi\pi$) and m($\pi K$) were considered, shown in figure 13.

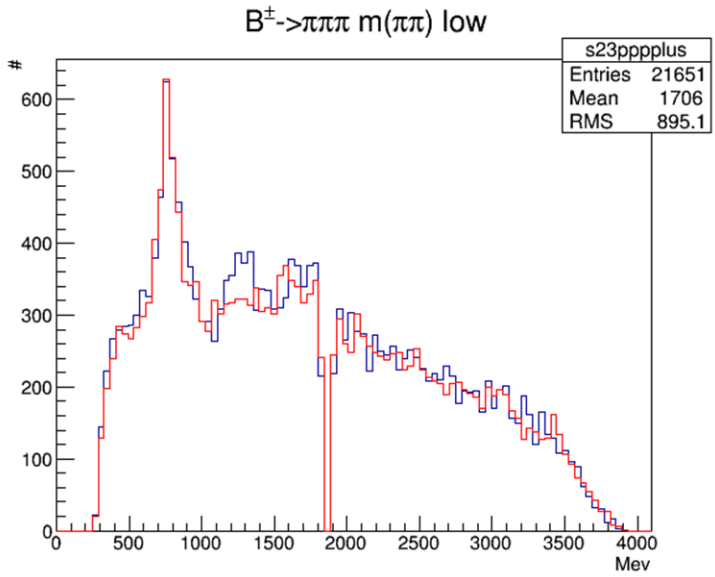

Figure 12: Low mass($\pi\pi$) pair, $\rho(770)$ resonance is present, this plot is shown in different style and scale to apreciate the differences between B+ and B-. (Red line for B+ and blue line for B-)

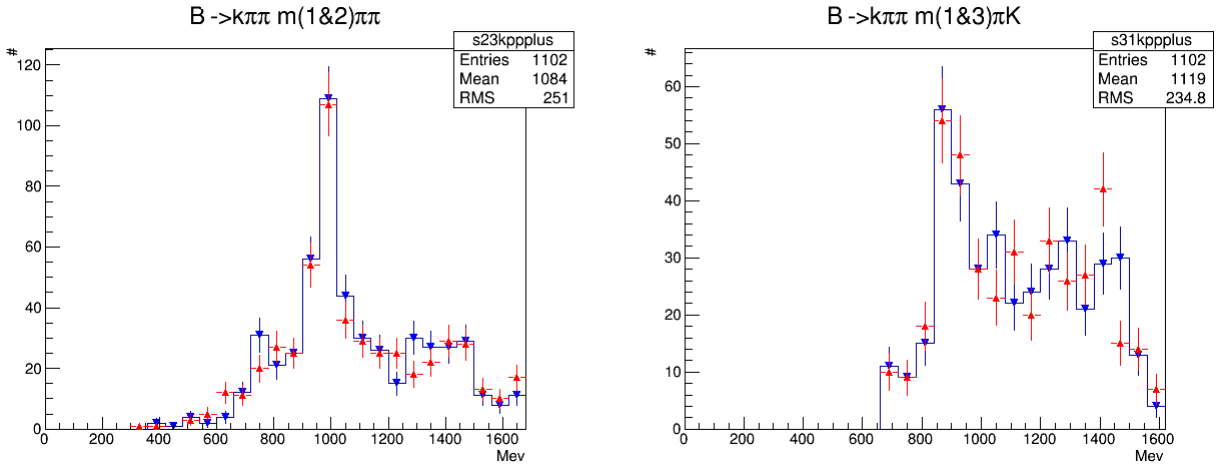

Figure 13: To the left m($\pi\pi$), where $f_0(980)$ and $\rho(770)$ resonance peaks are clearly seen. To the right m(πK), where $K^*(892)$ resonance is shown.

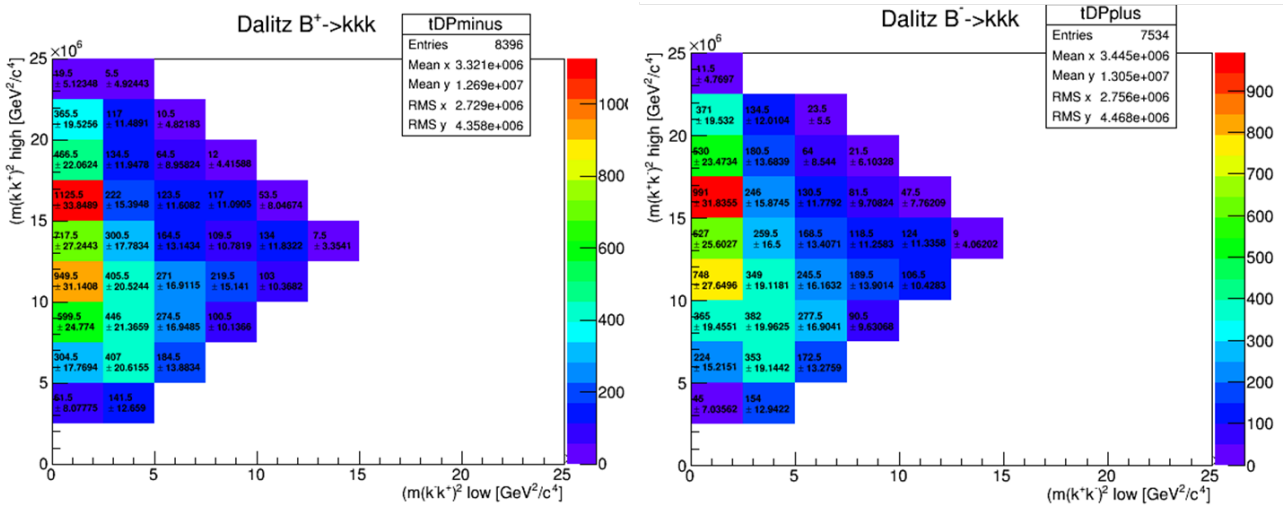

Figure 14: Daltiz Plots for $B^{\pm} \to K^{\pm}K^{+}K^{-}$ decay, significant diferences in the number of events can be seen between 0-2.5 GeV in the X axis (where $\phi(1020)$ resonance is located) and below 12.5 GeV in the Y axis.

2.4 Regional Asymmetries

Since the global asymmetries were found to be very small, regional asymmetries will now be considered, to this end, Dalitz plots were made from the square power of these pair masses (m^2 of the defined intermediates states described before) placed in each axis of a two dimensional histogram. Resonances appear as bands of events in the Dalitz plot, position and size of bands depends on the mass of each resonance and exact pattern of events is determined by interference between the various contributing states, for more details see Appendix A. Using high resolution Dalitz plots (>50 bins in each axis) was useful to spot cuts made in pair masses (J/ψ and D^0 contributions) and spot exact location of resonances involved, lower resolution (10 bins in each axis) for spotting differences between changed B mesons.

Dalitz plots were produced using poisson errors (low statistics per bin, generally <300 events per bin), $\sigma = \sqrt{N}$, for each decay channel (mass spectra region between 5240-5320 MeV, using natural units $c = 1$ from now on) and then background subtracted. This subtraction was done by choosing a region between 5400 and 5560 MeV (160 MeV width) which corresponds to combinatorial background (see figures 9-11) because of the significant overlap in the 5240-5320 MeV region. 4-Body decay background was ignored since the overlap was negligible. Since combinatorial background region has twice the width of original region for Dalitz plots, a normalization procedure was made before subtraction, multiplication by 1/2, taking into account errors of subtraction. Dalitz plots after background subtraction are shown in figures 14, 15 and 16, where the number of events and errors per bin are presented.

From the Dalitz plots, Asymmetry plots were made to look for regional asymmetries in phase space by using equation 5 and treating errors as binomial for the division given the low statistics,

$$\sigma^2 = \left| \frac{\left(1. - 2.\frac{n_1}{n_2}\right) e_1^2 + \frac{n_1^2}{n_2^2} e_2^2}{n_2^2} \right| ,$$

where the following mapping has been made to use the error formulae above, from equation 5:

$$Asy = \frac{(\frac{N^- - N^+}{N^- + N^+} + 1)}{2} \to \frac{N^-}{N^- + N^+} ,$$

then N^- corresponds to n_1 and $(N^- + N^+)$ to n_2. Hence, to get the error from the mapping back to original equation 5, it was multiplied by 2. The resultant asymmetry plots are shown in figures 17, 18 and 19, where the number of events and errors per bin are presented.

To compute the value of real regional asymmetries (signal events), the circled regions in the asymmetry plots were choosen to produce mass plots because of their overall statistical significance. In the case of $B^{\pm} \to \pi^{\pm}\pi^{+}\pi^{-}$, a wider

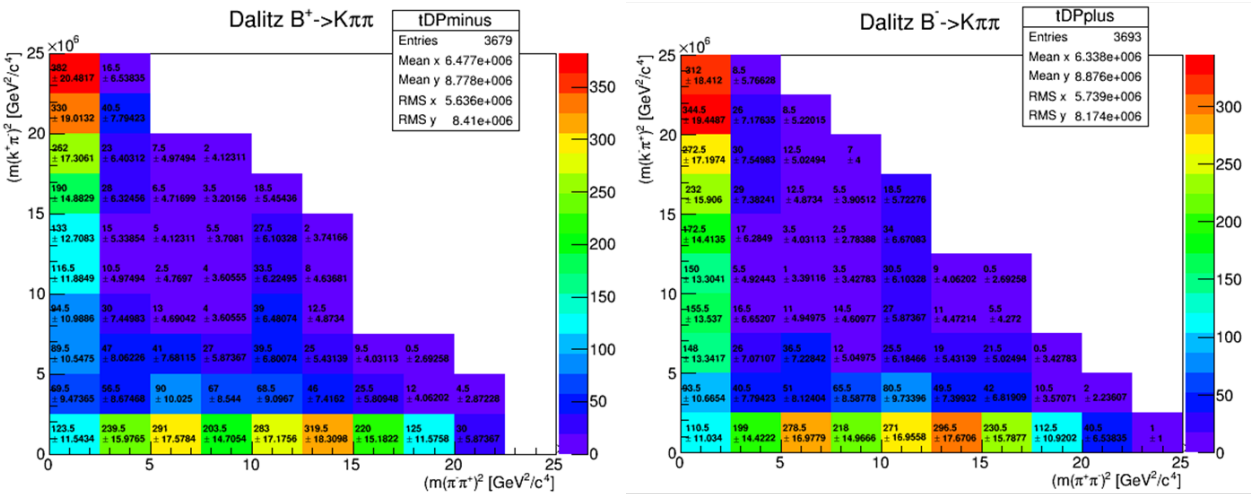

Figure 15: Daltiz Plots for $B^{\pm} \to K^{\pm}\pi^{+}\pi^{-}$ decay, significant diferences in the number of events can be seen between 0-2.5 GeV (where $f_0(980)$ and $\rho(770)$ resonances are located) in the X axis and 10-15 GeV in the Y axis. Also $K^{*}(892)$ interference pattern can be seen between 0-2.5 GeV in the Y axis.

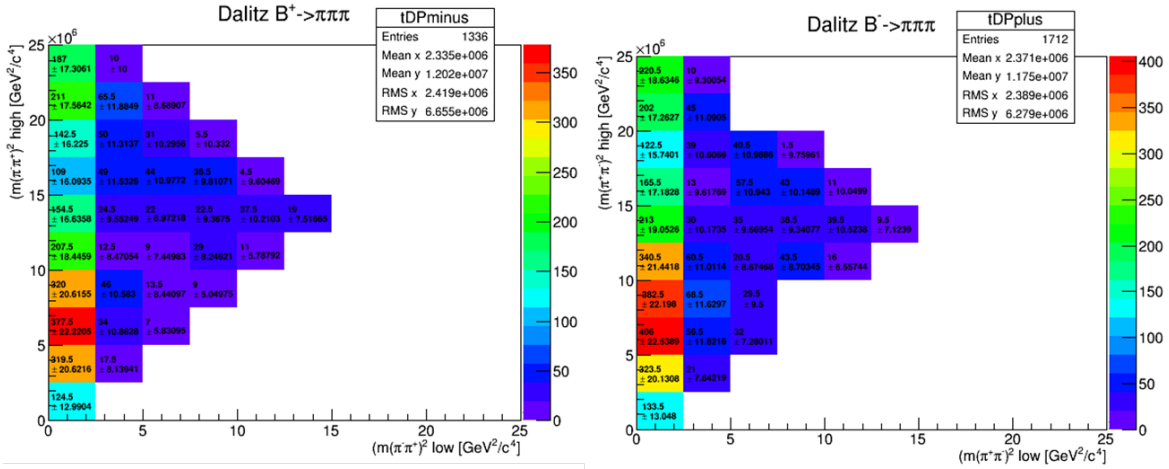

Figure 16: Daltiz Plots for $B^{\pm} \to \pi^{\pm}\pi^{+}\pi^{-}$ decay, significant diferences in the number of events can be seen between 0-2.5 GeV (where $\rho(770)$ is located) in the X axis and 5-10 GeV in the Y axis.

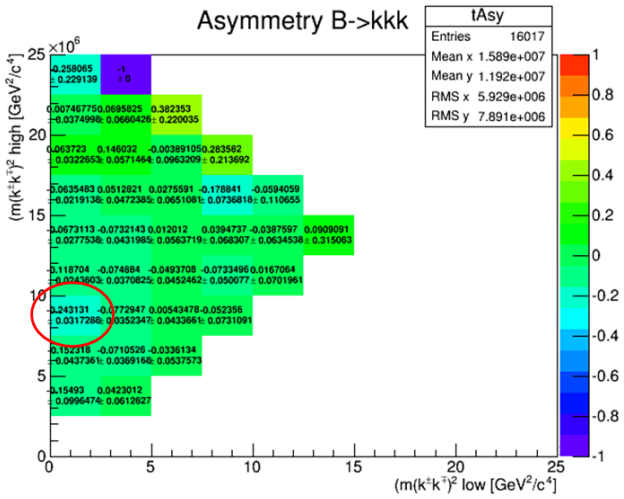

Figure 17: Asymmetry plot for the $B^{\pm} \to K^{\pm}K^{+}K^{-}$ decay, the area circled has an asymmetry of 24% with a significance of 7.7 sigma which is quite remarkable.

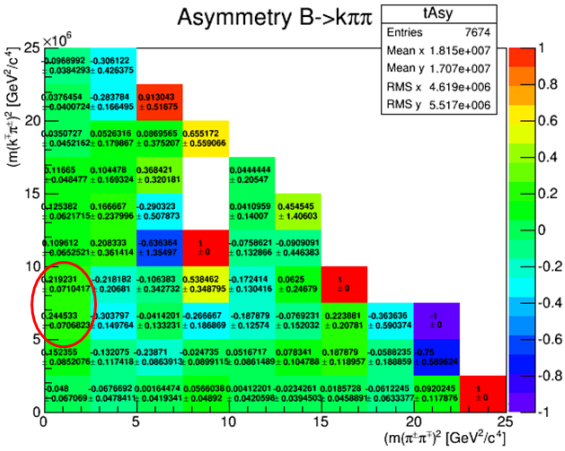

Figure 18: Asymmetry plot for the $B^{\pm} \to K^{\pm}\pi^{+}\pi^{-}$ decay, the area circled has an asymmetry of 22% and 24% with a significance of 3.1 and 3.5 sigma respectively.

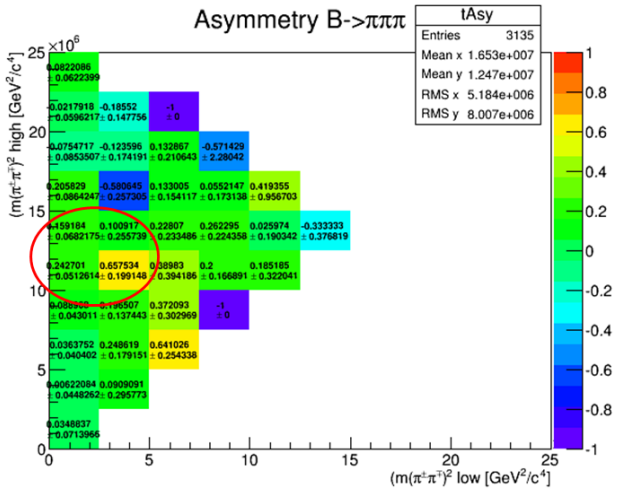

Figure 19: Asymmetry plot for the $B^{\pm} \to \pi^{\pm}\pi^{+}\pi^{-}$ decay, the lower region in the circled area has an asymmetry of 24% and 66% with a significance of 4.7 and 3.3 sigma respectively.

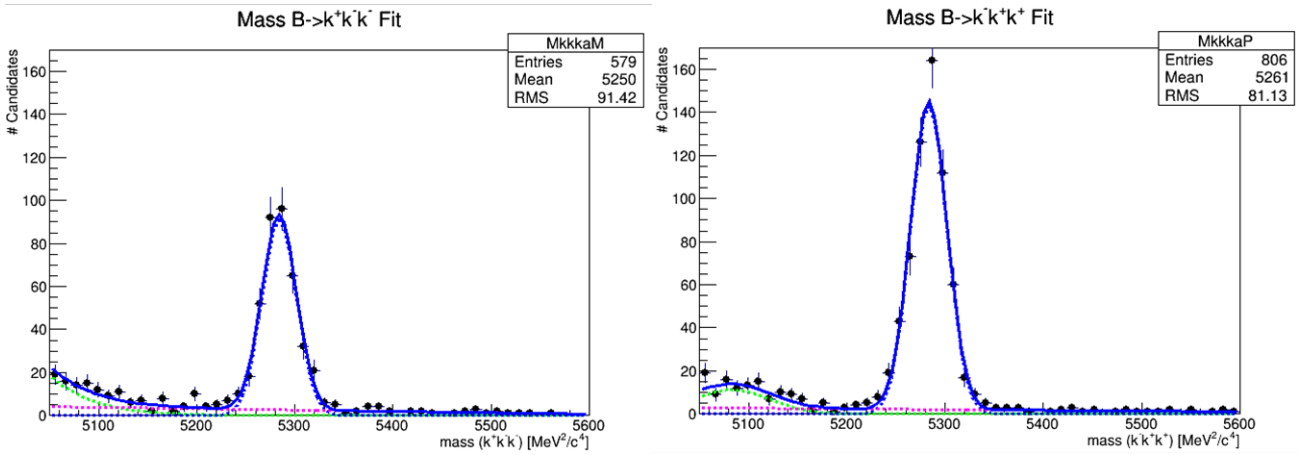

Figure 20: Invariant mass spectra of $B^{\pm} \to K^{\pm}K^{+}K^{-}$ decays in the region 0-2.5$m^2(KK)$ low GeV^2/c^4 and 7.5-10 $m^2(KK)$ high GeV^2/c^4, significant asymmetry of -0.246 ± 0.056.

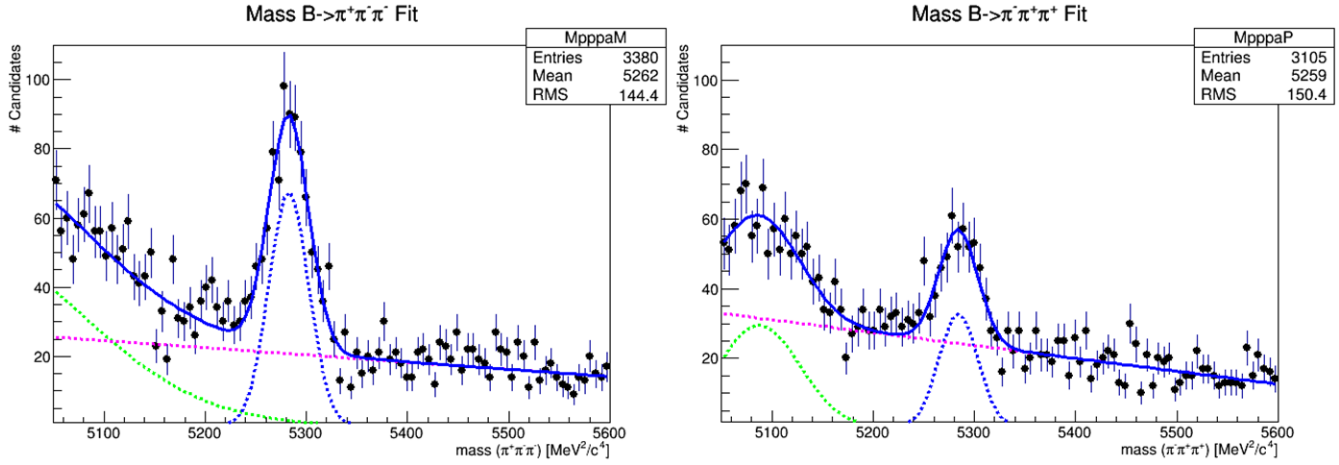

Figure 21: Invariant mass spectra of $B^{\pm} \to \pi^{\pm}\pi^{+}\pi^{-}$ decays in the region 0-5 $m^2(\pi\pi)$ low GeV^2/c^4 and 10-15 $m^2(\pi\pi)$ high GeV^2/c^4, significant asymmetry of -0.355$\pm$0.088.

region was choosen given the scarce number of events. The same fitting procedure for the global asymmetry was used (selection of functions to represent mass peak and background). The computed regional asymmetries are quite large, -0.246 ± 0.056 ($B^{\pm} \to K^{\pm}K^{+}K^{-}$), -0.355$\pm$0.088 ($B^{\pm} \to \pi^{\pm}\pi^{+}\pi^{-}$) and -0.446 ± 0.118 ($B^{\pm} \to K^{\pm}\pi^{+}\pi^{-}$). and are shown in figures 20, 21 and 22.

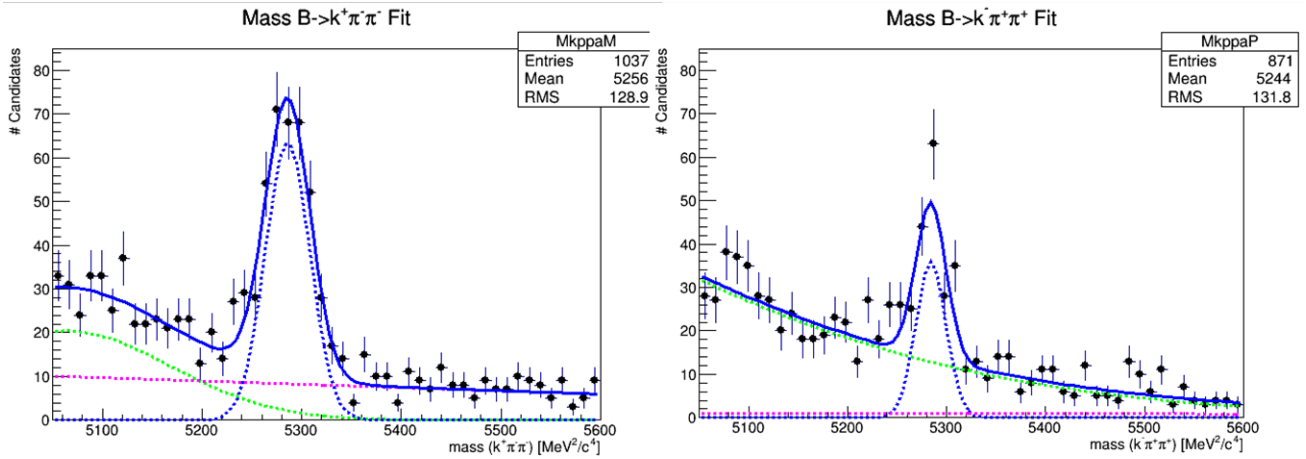

Figure 22: Invariant mass spectra of $B^{\pm} \rightarrow K^{\pm}\pi^{+}\pi^{-}$ decays in the region 0-2.5 $m^2(\pi\pi)\ GeV^2/c^4$ and 5-10 $m^2(K\pi)\ GeV^2/c^4$, significant asymmetry of -0.246 ± 0.056.

3 Laboratory experiment development

Some foundation material has been made for the future experiment to replace current particle physics experiment that uses DØ data. Students will be provided with a simplified version of the data set used fot this report in terms of variables and some additional pre-applied cuts. They will have to be able to produce results in 8 weeks time, just as current experiments. Students will have to choose one of the decay channels studied above and produce similar plots to get values of global and regional asymmetries and see for themselves evidence of CP violation.

- **Lab Script Draft**: This was produced using a very similar format that current lab scripts have. It has a theoretical introduction, a general description of the LHCb experiment, a general description on how the data analysis will be done and 2 appendices describing programming technicalities and information about Dalitz Plots.

- **Example Program**: An example program has been developed that produces a histrogram of momentum in X axis of one of the resultant particles after decay of B meson and saves it in a .root file. A similar program is provided to current students working on those experiments. The given program will treat variables differently since nTuples are saved in tree like structure, quite different from what they have now and they may not have a montecarlo simulation of the events. They will use the program for the data analysis and they may use macros for plotting and fitting histograms.

- **Demonstrator support plots**: Since the demonstrators are not necessarily experts in particle physics and even less in the study of CP violation of B mesons. Many of the plots produced for this study will be handed out to them. They may be used as a guide to check whether students are making sensible plots or progress with their experiment.

4 Discussion

Decay channels analyzed for this project were originally 2, $B^{\pm} \rightarrow K^{\pm}\pi^{+}\pi^{-}$ and $B^{\pm} \rightarrow K^{\pm}K^{+}K^{-}$. When sensible CP asymmetry results were obtained for those channels, then other possible decay channels were also analyzed, , $B^{\pm} \rightarrow K^{\pm}K^{+}\pi^{-}$ and $B^{\pm} \rightarrow \pi^{\pm}\pi^{+}\pi^{-}$. These were studied in recently published papers, [7](published first) and [9], their results were being reproduced in this project. Decays channels involving same particles gave the best results since it was quite simple to make the analysis with the hypothesis that all resultant particles have the same mass. This was balanced by the fact that intermediate states had to be ordered according to high-low mass for the production of Dalitz Plots. The $B^{\pm} \rightarrow K^{\pm}\pi^{+}\pi^{-}$ and $B^{\pm} \rightarrow K^{\pm}K^{+}\pi^{-}$ decay channels were more challenging because when making the hypothesis for different particle masses, events were not as abundant as the other channels and the background signals were particularly more complex to represent as functions for fitting, specially $B^{\pm} \rightarrow K^{\pm}K^{+}\pi^{-}$.

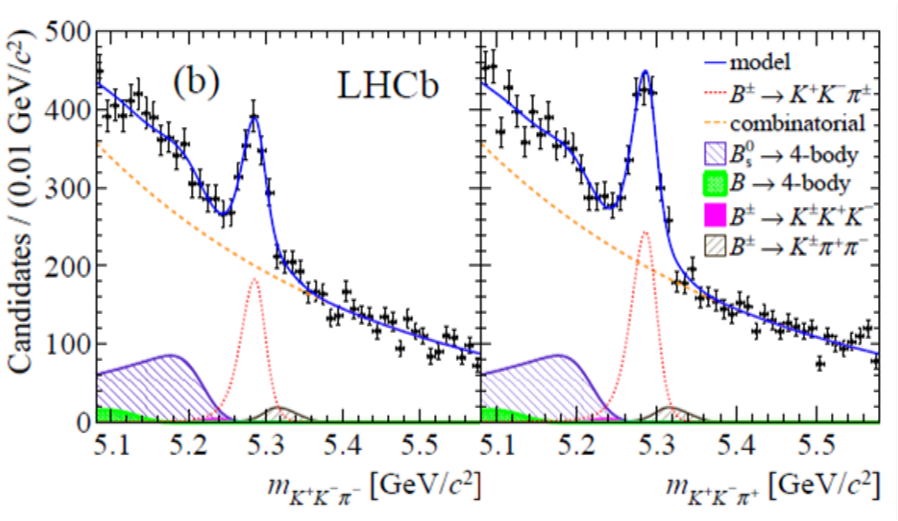

Figure 23: Invariant mass spectra of $B^\pm \to K^\pm K^+\pi^-$ decay channel. It was a very complex background. Reproduced from [9].

For the selection cuts, pre-applied cuts had to be identified first since it was noticed that some where applied when a invariant mass plot of B meson was produced. These were identified by plotting some of the given variables given in the nTuples as histograms to check were cuts were made, see figure 7. Then, PID cuts were identified as the strongest one to be applied, giving >90% reduction in signal events and this will be the main task for students doing the future experiment.

In the calculation of global asymmetries, fitting was crucial to get the number of signal events from the background. Simple functions were used since students will not have time to model more complex and appropiate functions to represent background. The best agreement was found in the $B^\pm \to K^\pm K^+K^-$ decay with previous studies, -0.053 ± 0.007 obtained compared to -0.043 ± 0.009 from paper . Decay channels involving pions have significant 4-Body decay background. When $B^\pm \to K^\pm K^+\pi^-$ was being analyzed, it was clear that the background was way too complex to be modelled (very significant overlap of 4-Body decays and combinatorial instead of just being combinatorial as the other decays) and was dropped as a possible decay channel for students to study, see figure 23. Then the project was centred in the remaining 3 decays.

When regional asymmetries were being analyzed in the Dalitz and Asymmetry plots, a plot of statistical significance, that is, asymmetry/error was very helpful for the selection of regions in phase space where CP asymmetry is large and with low uncertainty. Hence, this will be part of students work in order to select those significant phase space regions and produce invariant mass plots of B meson to spot these quite large asymmetries. They will be suggested to work with low resolution histograms, that is, with bins per axis <25 to easily spot those regions. In this project, 5, 7, 10 and 25 bins per axis were produced. Resonances were more easily spotted in 25x25 bins, 10x10 bins was the best for spotting asymmetries while looking also at the errors per bin. Lower resolution plots increasingly washed out the asymmetries, although, $B^\pm \to K^\pm K^+K^-$ decay still had >5 sigma significance even at 5x5 bins, see figure 24.

5 Conclusions

It was demonstrated that sensible results can be obtained for CP asymmetry in charmless B meson decays, hence it is a viable as a 3rd Year Lab Experiment to be done by students in 8 weeks time. They will have to choose one decay channel, is is suggested that they choose just $B^\pm \to K^\pm K^+K^-$ and $B^\pm \to \pi^\pm\pi^+\pi^-$ as general options and perhaps leaving $B^\pm \to K^\pm\pi^+\pi^-$ as a possibility for enthusiastic and able students warning them of the difficulties and considering compensation. The best result were obtained from $B^\pm \to K^\pm K^+K^-$ decay channel as discussed above. Different student groups could be assigned different decay channels. Students will learn that global CP asymmetries can be quite small, but when they study regional phase space regions, these asymmetries can become quite large for their amazement. Given the short time they have to do the experiment, they may also be given functions to deal

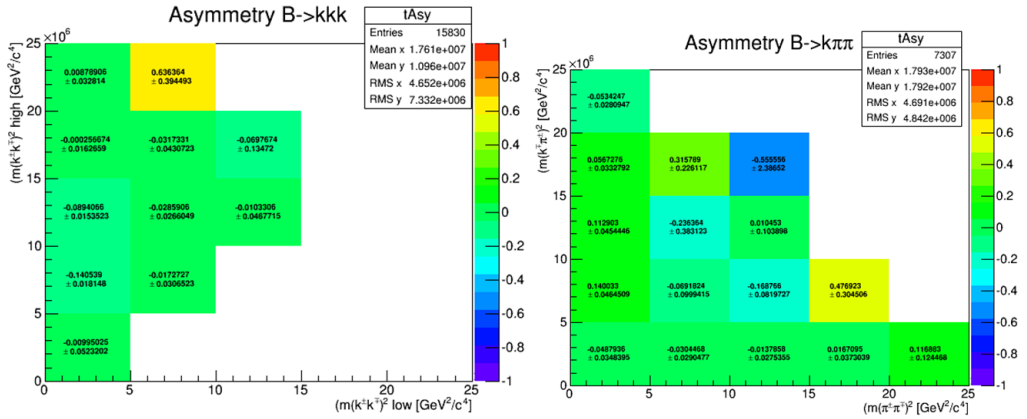

Figure 24: Left panel, asymmetry plot for the $B^{\pm} \to K^{\pm}K^{+}K^{-}$ decay, the area between 0-5 GeV in X axis and 5-10 GeV in Y axis has an asymmetry of 14% with significance of 7.7 sigma. Right panel, asymmetry plot for the $B^{\pm} \to K^{\pm}\pi^{+}\pi^{-}$ decay, same area, with an asymmetry of 14% with significance of 3 sigma.

with binomial errors and productions of asymmetry plots, these were time consuming when working on the project. The fitting of the mass plots is more complex than current experiment given the different sources of background, in a programming context, but there are examples available in Root documentation, an example could be provided.

References

[1] Modern Particle Physics, Mark Thompson, Cambridge 2013.

[2] A. Sakharov, Violation of CP Invariance, C Asymmetry, and Baryon Asymmetry of the Universe, Pisma Zh. Eksp. Teor. Fiz. 5 (1967) 32. 11

[3] I. J. R. Aitchison and A. J. G. Hey, Gauge Theories in Particle Physics, vol. 1 of Graduate Student Series in Physics, Taylor & Francis, 3rd ed., 2003.

[4] CP violation measurement in B± → K±π+π− and B± → K±K+K− decays in 2011 data, I. Bediaga1, A. Gomes2, J. Helder2, A. Massafferri1, J. M. de Miranda1, I. Nasteva1, J. Otalora2, F. Rodrigues1. 1 Centro Brasileiro de Pesquisas Fısicas, Brazil. 2 Universidade Federal do Rio de Janeiro, Brazil.

[5] LHCb collaboration, A. A. Alves Jr. et al., The LHCb detector at the LHC, JINST 3 (2008) S08005.

[6] The LHCb RICH Group, Performance of the LHCbRICH detector at the LHC, EPJC (2012) arXiv:1211.6759.

[7] Measurement of CP Violation in the Phase Space of B± → K±π+π− and B± → K±K+K− Decays. R. Aaij et al.* (LHCb Collaboration). PRL 111, 101801 (2013).

[8] A Modern Introduction to Particle Physics (3rd Edition), Fayyazuddin & Riazuddin

[9] Measurement of CP violation in the phase space of B± → K±K+π− and B± → π±π+π− decays. R. Aaij et al.* (LHCb Collaboration). PRL 112, 011801 (2014).

A Dalitz Plots

Dalitz plots are representations of the phase space of 3-body decays involving mostly spin 0 particles and named after Richard Dalitz (1925–2006). The main advantage of Dalitz plots is ability to exploit inference between different resonances, see figure 23. They show intuitive connection between visualisation and kinematics which can be completely described using two variables.

Consider a 3-body decay, treating the problem in centre of mass frame and calling the centre of mass energy M, the mass of the parent particle, also calling $\mathbf{p}_1$, $\mathbf{p}_2$ and $\mathbf{p}_3$ the momenta and E_1, E_2 and E_3 the energies of the three child particles. The following constraints apply:

- momentum conservation, $\mathbf{p}_1 + \mathbf{p}_2 + \mathbf{p}_3 = 0$
- energy conservation, $E_1 + E_2 + E_3 = M$.

The phase space volume for a three-body system, ignoring constant factors is [8]:

$$\propto \int \frac{d^3p_1}{E_1}\frac{d^3p_2}{E_2}\frac{d^3p_3}{E_3}\delta(E_1+E_2+E_3-M)\delta^3(\mathbf{p}_1+\mathbf{p}_2+\mathbf{p}_3)$$

Now integrating over $\mathbf{p}_3$ using the δ^3 delta function,

$$\propto \int \frac{1}{E_1E_2E_3}d^3p_1d^3p_2\delta(E_1+E_2+E_3-M)$$

Integration over solid angles of vectors $\mathbf{p}_1$ and $\mathbf{p}_2$ by fixing θ_{12} angle between those vectors and integrating over θ_1, ϕ_1 and ϕ_2 :

$$\propto \int \frac{1}{E_1E_2E_3}4\pi p_1dp_1 2\pi p_2^2dp_2d\cos(\theta_{12})\delta(E_1+E_2+E_3-M)$$

Using momentum conservation, $p_3^2 = p_1^2+p_2^2+2p_1\cdot p_2\cos\theta 12$ and differentiating it by keeping p_1 and p_2 constant , $2p_3dp_3 = 2p_1p_2d\cos\theta 12$ and replacing in the integral above:

$$\propto \int \frac{p_1dp_1p_2dp_2p_3dp_3}{E_1E_2E_3}\delta(E_1+E_2+E_3-M)$$

Then by differentiating $E_i^2 = p_i^2 + m_i^2 \rightarrow p_idp_i = E_idE_i$ and replacing back in the above integral and using the remaining delta function for integration:

$$\propto \int dE_1dE_2dE_3\delta(E_1+E_2+E_3-M) \propto \int dE_1dE_2 \propto \int dm_{23}^2dm_{13}^2$$

Which shows that m_{23}^2 and m_{13}^2 fully defines the system, see Figure 7:

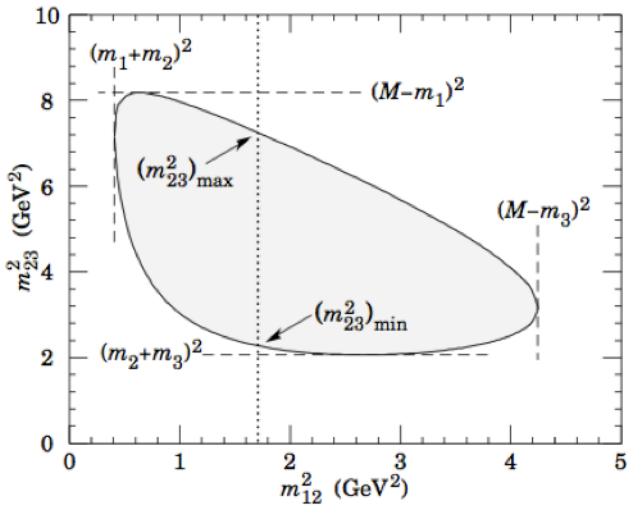

Figure 25: Taking $m_{12}^2 = (E_1 + E_2)^2 - (\mathbf{p}_1 + \mathbf{p}_2)^2 = (M - E_3)^2 - \mathbf{p}_3^2 = M^2 + m_3^2 - 2ME_3$, since all of the momenta and energies are related, picking m_{12}^2 and m_{23}^2, fully defines the system. Reproduced from [8].